Progress In Electromagnetics Research B, Vol. 57, 191–205, 2014

Investigation of the Effect of Ionospheric Gradients on GPS Signals in the Context of LAAS

Vemuri Satya Srinivas[1], Achanta D. Sarma[1, *], Ammana Supraja Reddy[2], and Desireddy Krishna Reddy[1]

Abstract—Local Area Augmentation System (LAAS) is expected to enable the pilots to guide the aircraft more precisely and safely into busy airports even in poor visibility conditions. The anomalous low and equatorial latitude Ionosphere is severe threat to the LAAS system. To characterize the anomalous ionospheric gradients, the performance of an ionospheric threat model is evaluated. In our investigation, in contrast to the reported work available in the open literature, smoothed code phase measurements are used in the threat model to obtain precise ionospheric time delay. The three key parameters of the threat model gradient slope (mm/km), width (km) and front speed (m/s) are used in the analysis. Further, geometry screening using Maximum Ionosphere Induced Error in Vertical (MIEV) as a key parameter is carried out to identify the stationary gradients and its impact on system performance for CAT-I operations. A maximum ionospheric gradient of 355.74 mm/km over a distance of approximately 75 km is reported at mid latitudes. Whereas, in our findings at low/equatorial latitudes even within a distance of approximately 4 km a maximum gradient of 460 mm/km is observed, which is comparatively very high. Our results show that, there is necessity to enhance upper bound for the ionospheric gradients threat space over low latitudes.

1. INTRODUCTION

The GPS satellites transmit two spread spectrum pseudo-random noise (PRN) radio signals on L_1 (1575 MHz) and L_2 (1227 MHz) frequencies with power level of -128 dBm and -134 dBm respectively. The L-band signals confront time delay effect, while passing through the ionosphere. Therefore, ionospheric time delay models are required to correct the effect of ionosphere on electromagnetic waves [1]. The vertical delay estimation due to the models at the user's Ionospheric Pierce Point (IPP) will be in error if any of the satellite signals get affected due to ionospheric irregularity. Especially, the ionosphere above the Indian subcontinent, which is located near the equatorial region, is highly volatile and varies both temporally and spatially [2–4]. In general the rate of change of Total Electron Content (TEC) over short distance ($\sim$100 km) is very small [5]. But, in presence of ionospheric gradients the TEC can change by tens of meters in just a few minutes [6]. Thereby causing significant difference in TEC experienced by users at short distances, even less than 45 km. Therefore, the effect of large ionospheric gradients is of major concern and of particularly important in context of GBAS. The U.S. LAAS is an example of GBAS. ICAO recommends LAAS for Precision Approach (PA) at or near the airports (ICAO Annex 10). Many countries started developing GBAS for PA procedures at major airports. The GBAS Category-I (CAT-I) PA is demonstrated at Newark (USA), but not yet operational due to technical and operational issues. In, Australia (Sydney international airport) and Brazil the CAT-I operations will be in effect in the upcoming years. As far as India is concerned, the GBAS pilot project is expected to start at Chennai international airport in the near future and later expected in all other major airports [7, 8].

Received 13 October 2013, Accepted 6 December 2013, Scheduled 9 December 2013

* Corresponding author: Achanta Dattatreya Sarma (ad_sarma@yahoo.com).

[1] Chaitanya Bharathi Institute of Technology, Gandipet, Hyderabad (A.P.) 500 075, India. [2] R&T Unit for Navigational Electronics, Osmania University, Hyderabad 500 007, India.

The occurrence of strong ionospheric gradients is a potential threat to the LAAS. Significant research work specific to ionospheric threat modelling and analysis for LAAS is realized by several authors at mid latitude regions [9, 10]. Whereas, not much work relevant to threat analysis is done on low/equatorial latitude ionosphere, which is characterized by intense irregularities, scintillation and ionospheric gradients etc.. As the ionosphere in equatorial and low altitude regions like India is very volatile, it is technically challenging for the GNSS systems to meet the precision approach requirements of aviation. Our investigations are likely to fill this gap.

For better evaluation, smoothed code observations for detecting the large ionospheric gradients are used, which is in contrast to the smoothing techniques reported in open literature [10]. The analysis is carried out to meet the CAT-I PA requirements for low latitude regions.

2. LOCAL AREA AUGMENTATION SYSTEM (LAAS) AND IONOSPHERIC GRADIENTS

LAAS is one such system that enables pilots to guide planes more precisely and safely into busy airports even in bad weather conditions.

LAAS comprises of a ground station with multiple GPS receivers at well surveyed locations, a VHF link and one or more pseudolites (PLs). A simplified block diagram of LAAS is shown in Figure 1. Pseudolites (PLs) are ground based transmitters that can provide similar navigation measurements as GPS satellites. The usage of PLs offers great flexibility in terms of geometry and signal availability, which will aid in attaining CAT-I/II/III. The ground station makes the differential corrections and then broadcast them on VHF frequencies along with an integrity message to aircrafts within a radius of 30 to 50 km.

The extreme ionospheric spatial decorrelation is a major threat to LAAS and can result in positioning error of 10 m and more [11]. The term ionospheric gradient is used to represent this phenomenon. The methods/techniques to calculate these gradients are 'time-step', 'station pair' and 'mixed-pair' methods [11, 12]. These three techniques are used to estimate the steepest gradients and to bound the ionospheric error for GNSS augmentation systems. Spatial gradients are of major concern especially in LAAS for category PA operations. In a typical LAAS scenario, the LGF should detect the risk associated with ionospheric gradients and has to exclude the anomalous ranging sources. Therefore, thorough investigations are required to study anomalous ionosphere for both quiet and disturbed conditions. The gradient analysis is performed using station-pair method, which is reliable

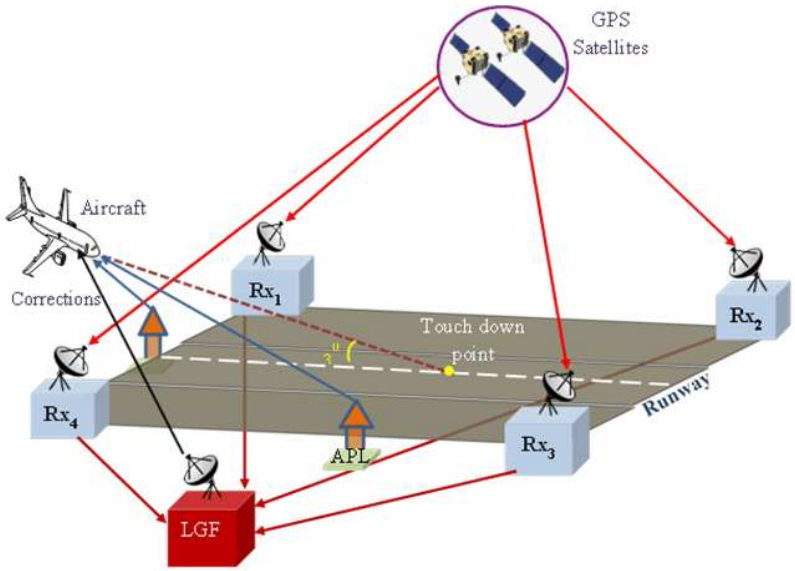

Figure 1. Block diagram of GBAS/LAAS.

for identifying the extreme spatial gradients.

2.1. Ionospheric Wave Front

An anomalous ionosphere gradient can be modeled as a linear semi-infinite wave front with constant propagation speed. The gradient is assumed to be a linear change in slant/vertical ionosphere delay between maximum and minimum delays. The spatial gradient (slope), width of the linear change in delay and the forward propagation speed of the wave front relative to the ground are the three key parameters in the LAAS ionosphere threat model (Figure 2). The threat model is expected to identify occurrence of ionospheric wave front by determining steepest gradients, width and its direction. Figure 3 illustrates typical LAAS scenario with ionospheric wave front. The spatial gradients are identified for the satellite visible to both the LGF and aircraft. The necessary computations for identification of ionospheric threat are carried out at LGF. The LGF will check all the visible satellites at every epoch for possible ionospheric anomaly and ensures the subset of satellites that are safe to use by an approaching aircraft. The bounds (sigma's) on the various errors such as multipath, troposphere, ionosphere etc., are also transmitted.

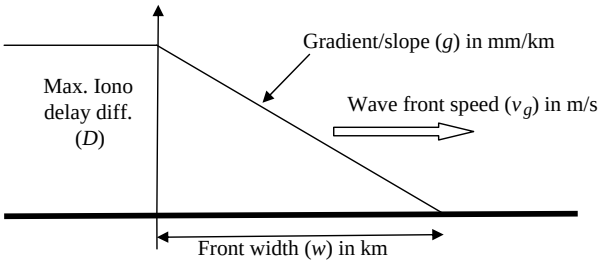

Figure 2. Illustration of ionospheric wave front.

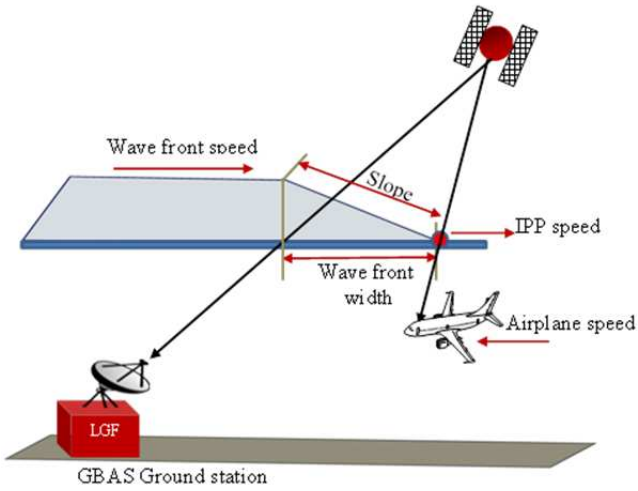

Figure 3. Illustration of ionospheric front in typical LAAS scenario.

The aircraft uses the LGF approved satellite geometries and range error (sigma's) to determine integrity by computing the protection levels. The work in this paper is limited to analysis of spatial gradients in the context of LAAS and to determine safe satellite geometries for CAT-I PA. Computation of protection levels is out of scope of this work, but briefly described in next section to highlight the significance of the work presented in this paper.

2.2. Ionospheric Wave Front Characteristics

The ionospheric wave fronts are classified as moving wave front and stationary wave front. During the precision approach the relative speed of aircraft with moving front determines, whether it is a "slow" or

Table 1. Typical range of ionospheric threat space parameters [14].

S. No.	Parameters	Typical Range
1.	Spatial gradient	4–450 mm/km
2.	Velocity of ionospheric wave front (V_{iono})	0–750 m/s
3.	Width of ionospheric wave front (W_{iono})	3–250 km

"fast" moving wave front [13]. The advantage of fast moving front is that the ionospheric anomaly can be detected much earlier at the LGF. Table 1 gives limits of slow and fasting moving wave fronts [14]. On the other hand, the stationary fronts impose severe threat to the LAAS user and are treated as worst case scenario and are mitigated through Geometry screening, with MIEV as key deciding parameter.

3. PROTECTION LEVELS

The Protection Levels (PLs) are bounds on residual errors that are caused due to thermal noise, multipath, nominal ionospheric and tropopsheric gradients with respect to airborne and reference receivers [15]. LAAS provides two types of protection levels, they are; Vertical Protection Level (VPL) and Horizontal Protection Level (HPL), which are function of satellite geometry. The considered satellite geometry is safe for positioning, if the calculated PLs are within the specified Alert Limits (ALs). The horizontal (H) and vertical (V) ALs for CAT-I/II/III precision approaches is given in 'GNSS Standards and Recommended Practices (SARPS)' ICAO document (2000). The VPL and HPL are calculated using the following expressions [16, 17],

$$\mathrm{VPL} = K_{MD}\sqrt{\left(\sum_{i=1}^{N} S_{v,\,i}^2 \times \sigma_i^2\right)} \tag{1}$$

$$\mathrm{HPL} = K_{MD}\sqrt{\left(\sum_{i=1}^{N} S_{y,\,i}^2 \times \sigma_i^2\right)} \tag{2}$$

where,

K_{MD}: Probability of missed detection.

$S_{y,i}$ and $S_{v,i}$: Horizontal and vertical component of projection matrix of ith ranging source.

σ_i^2: Error variance of each satellite in view of ith ranging source.

$$\sigma_i^2 \;=\; \sigma_{pr\_gnd,i}^2 \;+\; \sigma_{pr\_air,i}^2 \;+\; \sigma_{tropo,i}^2 + \sigma_{iono,i}^2 \tag{3}$$

In Eq. (3), the $\sigma_{pr\_gnd,i}^2$, $\sigma_{pr\_air,i}^2$, $\sigma_{tropo,i}^2$ and $\sigma_{iono,i}^2$ are the variances of ground error, airborne receiver error, troposphere error and ionosphere error respectively. Among them the $\sigma_{iono,i}$, is the function of standard deviation of nominal ionospheric spatial gradients (g_s), which is highly variable and can affect the integrity of LAAS user [18].

$$\sigma_{iono} \;=\; \sigma_{sg} \;\times (x_{aircraft} + 2\tau_s v_{aircraft}) \times sf \tag{4}$$

where,

σ_{sg}: Standard deviation of nominal ionospheric spatial gradient (mm/km) for ith ranging source.

$x_{aircraft}$: Distance between the LGF and aircraft (km).

τ_s: Time constant of single frequency GBAS carrier smoothing filter (s).

$v_{aircraft}$: Velocity of approaching aircraft (km/s).

sf: Slant or obliquity factor.

The slant factor (sf) is written as,

$$Sf = \sqrt{1 - \left(\frac{R_e \times \cos(\theta_{el})}{(R_e \;+ h_i)}\right)^2} \tag{5}$$

where,

R_e: Effective Radius of the earth (6378 km),

θ_{el}: Elevation angle (degrees) and,

h_i: Height of ionospheric shell (350 km).

In Eq. (4), the $x_{aircraft}$ is the distance between LGF and aircraft. The parameters $v_{aircraft}$ and τ_s are assumed as 70 m/s and 100 s respectively [14]. Usually in LAAS to mitigate the effect of spatial gradient, σ_{vig} ("vig" stands for 'vertical ionospheric gradient') of 4 mm/km is transmitted by the LGF to the user [19]. The σ_{vig} is expressed as [20],

$$\sigma_{\text{vig}} = \sigma_{sg} \times sf \tag{6}$$

But due to extreme spatial decorrelation of ionosphere at low and equatorial latitudes, 4 mm/km is not suitable. The details of other error variances ($\sigma^2_{pr\_gnd,i}$, $\sigma^2_{pr\_air,i}$ and $\sigma^2_{tropo,i}$) can be found elsewhere [21, 22]. The large ionospheric gradients that are observed in the propagation path of particular satellites are presented in results and discussion section.

4. THREAT SPACE PARAMETER ESTIMATION FOR LAAS

The ionospheric time delay is the largest and unpredictable source of error affecting the Required Navigation Performance (RNP) of aircraft navigation. The ionospheric mean conditions are dramatically affected because of variations in solar activity, which can endanger the integrity of GBAS systems.

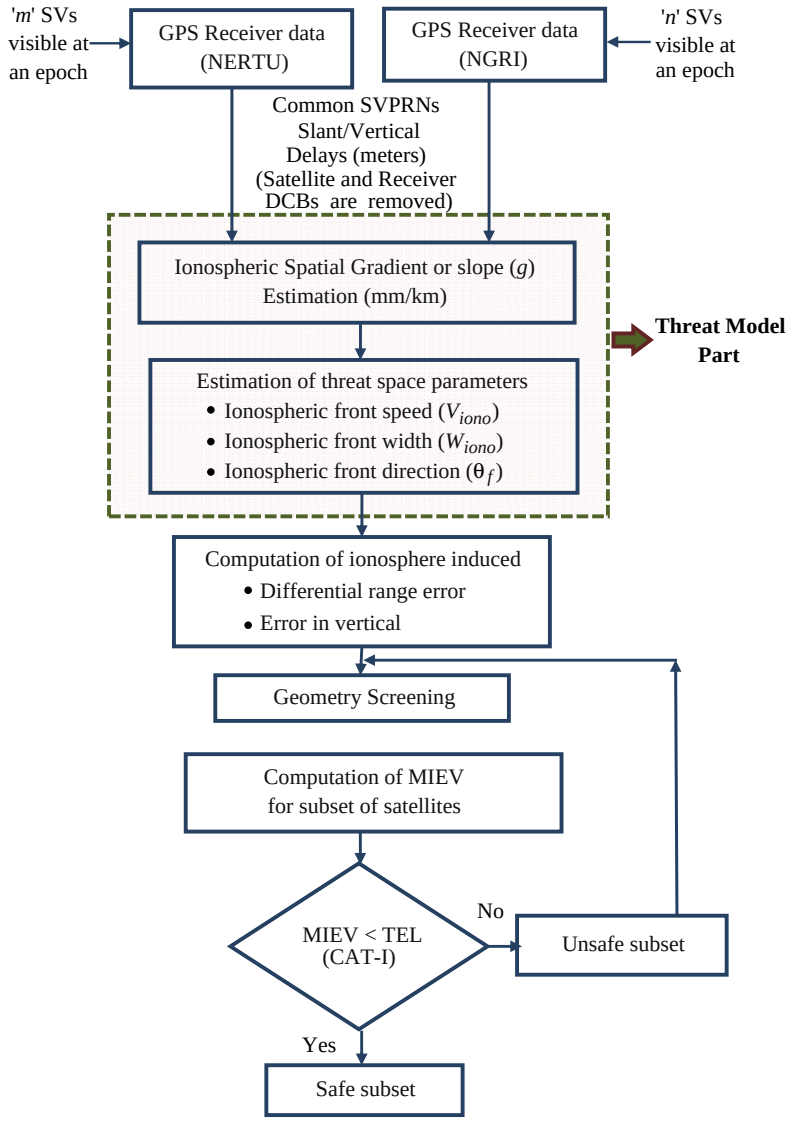

Figure 4. Flowchart for LAAS threat analysis.

Significant research work is done on ionospheric threat analysis specific to GBAS for Conterminous U.S. (CONUS) region. Theoretical back ground in respect of effect of anomalous ionospheric gradients on LAAS relevant to threat analysis can be found elsewhere [14, 24, 25]. But, the observations reported in these references were in the context of mid-latitude regions covering CONUS region. Relevant to development of ionospheric threat models and threat analysis specific to GBAS, not much significant work is done in low and equatorial latitude regions like India. As the ionosphere in these regions is volatile, it is technically challenging for the GNSS systems to meet the precision approach requirements of aviation. Therefore, an attempt is made in this aspect. The steps involved in identifying the gradient effected satellite and to obtain the safe satellite subset for navigation solution are illustrated in Figure 4.

The threat analysis in the context of LAAS requires a minimum of two GPS receivers with in a distance of 50 km. Therefore, the GPS data of two stations namely National Geophysical Research Institute (NGRI) and Research and Training Unit for Navigational Electronics (NERTU) of Hyderabad, which are spatially separated by a distance of 3.64 km is considered for the analysis. The steps involved in identifying the gradient effected satellite and to obtain the safe satellite subset for navigation solution are illustrated in Figure 5. The theoretical background including calculation of threat parameters with relevant mathematical expressions is discussed in this section.

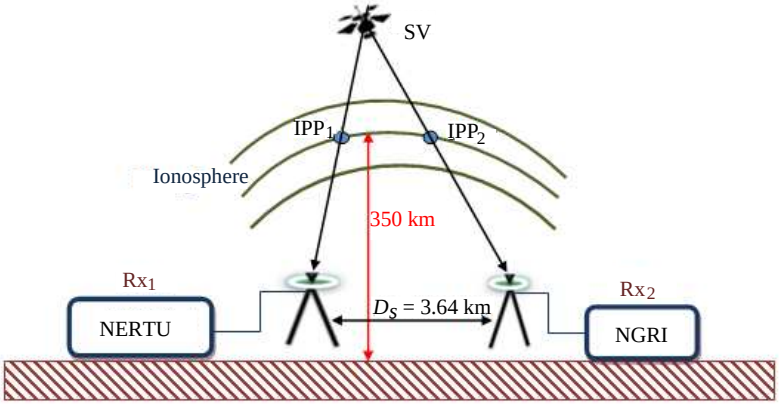

Figure 5. Illustration of station pair concept for estimation of spatial gradients.

4.1. Estimation of Ionospheric Spatial Gradient

Station pair method is used to estimate the ionospheric spatial gradients. This technique is suitable for LAAS scenario when compared to time step and mixed pair methods. Figure 5 illustrates the station pair concept. The spatial gradient (g_s) is given as [23],

$$g_s = \frac{\left| I^p_{d_{\mathrm{Rx}_1}} - I^p_{d_{\mathrm{Rx}_2}} \right|}{D_s} \ (\mathrm{mm/km}) \tag{7}$$

where,

$I^p_{d_{\mathrm{Rx}_1}}$ and $I^p_{d_{\mathrm{Rx}_2}}$: Slant ionospheric delay of the receivers Rx_1 and Rx_2 due to common visible satellite P.

D_s: Distance between the two receivers.

4.2. Estimation of Velocity and Width of Ionospheric Wavefront

Ionospheric front speed (V_{iono}) and width (W_{iono}) are required to characterize the gradient. Dividing the distance between the two stations by the time difference of occurrence of maximum delays at the two stations (Rx_1, Rx_2) gives ionospheric front speed. But, the front speed also includes the IPP velocity (V_{ipp}), which is an essential parameter required for estimation of width of the wave front. The velocity of IPP is the ratio of distance between successive IPP's of the satellite in view of the receiver, to the

difference in time of observations. So, the velocity of wave front, width and IPP velocity are given as [24],

$$v_{iono} = \frac{D_s}{\Delta t_{\mathrm{Rx}_1,\mathrm{Rx}_2}} \text{ m/sec} \tag{8}$$

$$\Delta t_{\mathrm{Rx}_1,\mathrm{Rx}_2}(\mathrm{Rx}_1 \neq \mathrm{Rx}_2) = \left| t_{peak_{\mathrm{Rx}_1}} - t_{peak_{\mathrm{Rx}_2}} \right| \tag{9}$$

$$W_{iono} = (V_{iono} - V_{\mathrm{IPP}}) \times t_g \tag{10}$$

$$V_{ipp} = \frac{D_{\mathrm{IPP}}}{t_{\mathrm{IPP}}} \tag{11}$$

where,

$t_{peak_{\mathrm{Rx}_1}}$: Time of occurrence of maximum ionospheric delay at station Rx_1 (sec).

$t_{peak_{\mathrm{Rx}_2}}$: Time of occurrence of maximum ionospheric delay at station Rx_2 (sec).

t_g: Time (sec) taken for linear change in ionospheric delay from maximum to minimum.

D_{IPP}: Distance between the IPP points at time t_1 and t_2 due to satellite in view (meters).

t_{IPP}: Difference of two time instants t_1 and t_2 (sec).

4.3. Calculation of Direction of Wave Front

The pictorial representation of the effect of ionospheric gradients on satellite signals is depicted in Figure 6.

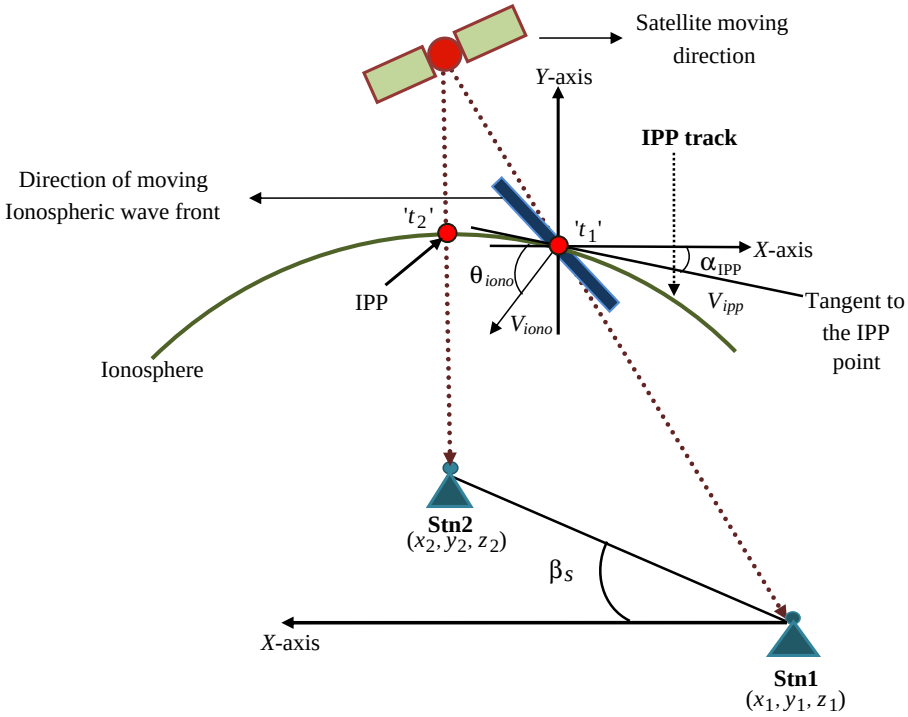

Figure 6. Illustration of ionospheric gradient and two stations scenario.

There are two stations with local coordinates (x_1, y_1, z_1) and (x_2, y_2, z_2) respectively. The ionospheric wave front and satellite in view are moving in opposite directions. The wave front sweeps over the stations 1 and 2 at time instants t_1 and t_2.

Though, two receivers' data is sufficient to estimate the ionospheric gradient and its speed, in general a third receiver is required to determine its direction. Ene et al. [25] developed a more generalized

method which aid in finding the direction of wave front even with two stations data [25]. The model is expressed as,

$$D_s \times \cos(\beta_s) = (V_{iono}\cos(\theta_{iono}) + V_{\text{IPP}}\sin(\alpha_{\text{IPP}})) \times \Delta t_{\text{Rx}_1,\text{Rx}_2} \tag{12}$$

where, α_{IPP} and θ_{iono} are the angles defined to determine IPP direction and wave front direction. Further, β_s is the angle between line joining two stations and x-axis. β_s is calculated from the 3-dimensional direction cosine rule of the vector algebra given as,

$$\beta_s = \cos^{-1}\left(\frac{(x_2 - x_1)}{\sqrt{\left((x_2 - x_1)^2 + (y_2 - y_1)^2 + (z_2 - z_1)^2\right)}}\right) (\text{deg}) \tag{13}$$

For calculating β_s angle, the coordinates of two receivers NERTU (1211955.4671 m, 5966555.9125 m, 1896150.2498 m) and NGRI (1208444.4559 m, 5966806.0124 m, 1897076.9818 m) are considered and obtained as 15.3°. In Eq. (12), the only unknown parameter for estimation of wave front direction (θ_{iono}) is IPP direction angle (α_{IPP}).

α_{IPP} is the angle between the IPP moving direction and normal direction of the front. The concept of line geometry is used to estimate α_{IPP} and is illustrated in Figure 7. The angle between the tangent and Line of Sight (LOS) is 90°, and the angle between line parallel to equatorial plane and LOS is angle of elevation [26]. Therefore, the direction of IPP is expressed as,

$$\alpha_{\text{IPP}} = 90^\circ - \theta_{el}\ (\text{deg.}) \tag{14}$$

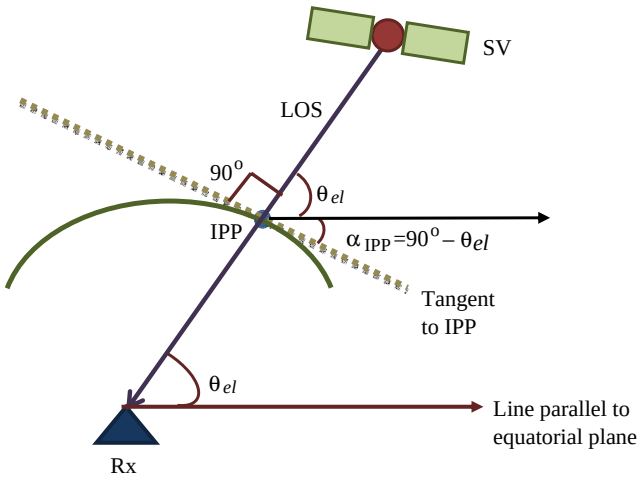

Figure 7. Illustration of IPP direction.

4.4. Calculation of Ionosphere Differential Range Error and Error in Vertical

The signal processing at the LAAS ground station consists of data checks to prevent transmission of misleading information to the aircraft. Thereby, the LGF broadcasts valid corrections for all approved satellites in view. The satellite specific differential range error (ε) and ionosphere induced error in vertical (IEV) are given as [15],

$$\varepsilon = \min\left[\frac{50}{W_{iono}}, \max(g_s)\right] \times (x_{aircraft} + 2\tau_s v_{aircraft})\ (\text{meters}) \tag{15}$$

$$\text{IEV} = |S_{vert_i} \times \varepsilon| \tag{16}$$

where, ε: Ionospheric induced differential range error (m).

In Eq. (16), S_{vert_i} is calculated from weighted least square projection matrix (S_p), which is given as,

$$S_p = \left((G_{el\_az})^T \times W_{ev} \times G_{el\_az}\right) \times (G_{el\_az})^T \times W_{ev} = \begin{bmatrix} S_{x1} & S_{x2} & \dots & S_{xn} \\ S_{y1} & S_{y2} & \dots & S_{yn} \\ S_{v1} & S_{v2} & \dots & S_{vn} \\ S_{t1} & S_{t2} & \dots & S_{tn} \end{bmatrix} \tag{17}$$

$$S_{vert_i} = S_{v,i} + (S_{x,i} \times \tan(\theta_{\mathrm{GPA}})) \tag{18}$$

$$G_{el\_az} = \begin{bmatrix} \cos(\theta_{el_1})\cos(\mathrm{Az}_1) & \cos(\theta_{el_1})\sin(\mathrm{Az}_1) & \sin(\theta_{el_1}) & 1 \\ \cos(\theta_{el_2})\cos(\mathrm{Az}_2) & \cos(\theta_{el_2})\sin(\mathrm{Az}_2) & \sin(\theta_{el_2}) & 1 \\ \vdots & \vdots & \vdots & \vdots \\ \cos(\theta_{el_n})\cos(\mathrm{Az}_n) & \cos(\theta_{el_n})\sin(\mathrm{Az}_n) & \sin(\theta_{el_n}) & 1 \end{bmatrix} \tag{19}$$

$$W_{ev} = \begin{bmatrix} \sigma_1^2 & 0 & \dots & 0 \\ 0 & \sigma_2^2 & \dots & 0 \\ 0 & 0 & \dots & 0 \\ 0 & 0 & \dots & \sigma_n^2 \end{bmatrix}^{-1} \tag{20}$$

where, $n \times 4$ observation matrix (G_{el_az}) is estimated using LOS elevation (θ_{el}) and azimuth (Az) in up-east-north (UEN) reference frame. W_{ev} is the $n \times n$ weighted matrix defined as a function of error variance of each satellite in view. θ_{GPA} is the Glide Path Angle (GPA), which is normally referred as 3°.

4.5. Maximum Ionospheric Error in Vertical (MIEV)

The calculation of Maximum Ionospheric Error in Vertical (MIEV) is required to check the integrity of subset of satellites to be used for navigation solution. The MIEV is calculated as [11],

$$\mathrm{MIEV} = |S_{vert_i}\varepsilon| + K_{MD}\sqrt{\sum_{i=1}^{N} S_{v,i}^2 \sigma_i^2} \tag{21}$$

In the equation, K_{MD} multiplier is the missed detection probability which is defined in LAAS Signal-in-Space (SIS) integrity and continuity requirements. The K_{MD} value depends on the number of receivers used in the LAAS operation. In the present example, two receivers are used for estimating ionospheric gradients. Therefore, K_{MD} value of 2.935 is chosen [22]. The MIEVs calculated for the subset of satellites at every instant are compared with the maximum vertical Total Error Limit (TEL) of about 28.78 m, which is allowable at the decision height (DH) of 200 ft for CAT-I precision approach. The satellite geometries with MIEV greater than aforesaid TEL are not considered by the airborne receiver for navigation solution.

5. RESULTS AND DISCUSSION

The GPS data corresponding to dual frequency GPS receivers of NERTU (Make: Novatel, Model: DL4plus) and NGRI (Make: Leica model: GRX1200GGPRO) is used for the analysis. As the dual frequency GPS receiver at NERTU is operational from year 2008, the data from 2008 to 2012 is investigated on the availability basis. The selected instances of satellites affected with large gradients are presented. Initially, the effect of anomalous ionosphere on GPS satellite signals for normal ionospheric conditions is perceived. The analysis is carried out for a typical day (02nd October 2008, $2 \leq \mathrm{Kp} \leq 4$). Figure 8 shows the spatial gradients observed for SVPRN 2 during normal ionospheric conditions. The minimum spatial gradient is 112 mm/km (15.8 Hrs LT) and maximum spatial gradient is 126 mm/km (20.63 Hrs LT). Figure 9 depicts the slant ionospheric spatial gradients observations for other satellites with visibility more than 3 hours on 2nd October 2008.

The satellite specific slant ionospheric spatial gradients are multiplied with the slant factor to measure the vertical ionospheric gradient. The slant factor varies inversely with elevation angle. Its

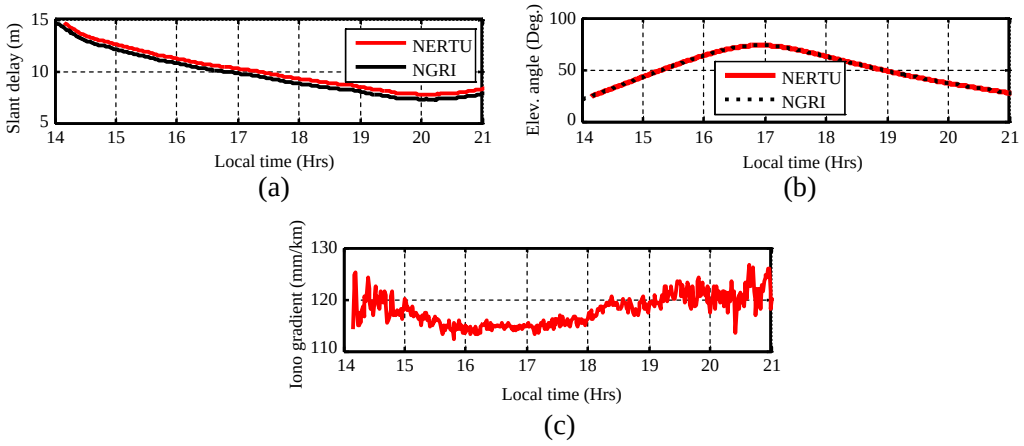

Figure 8. Local time versus (a) slant ionospheric delay, (b) elevation angle, (c) slant ionospheric spatial gradient of SVPRN 2.

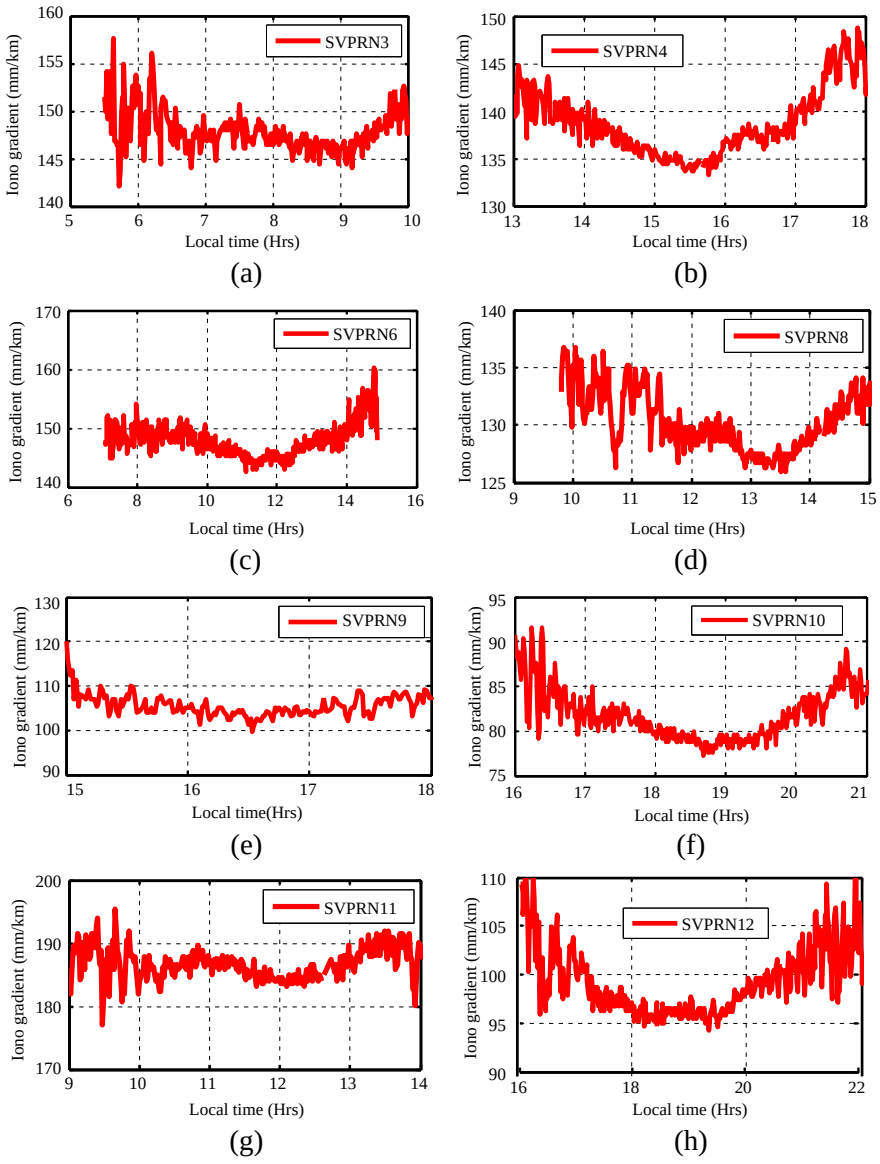

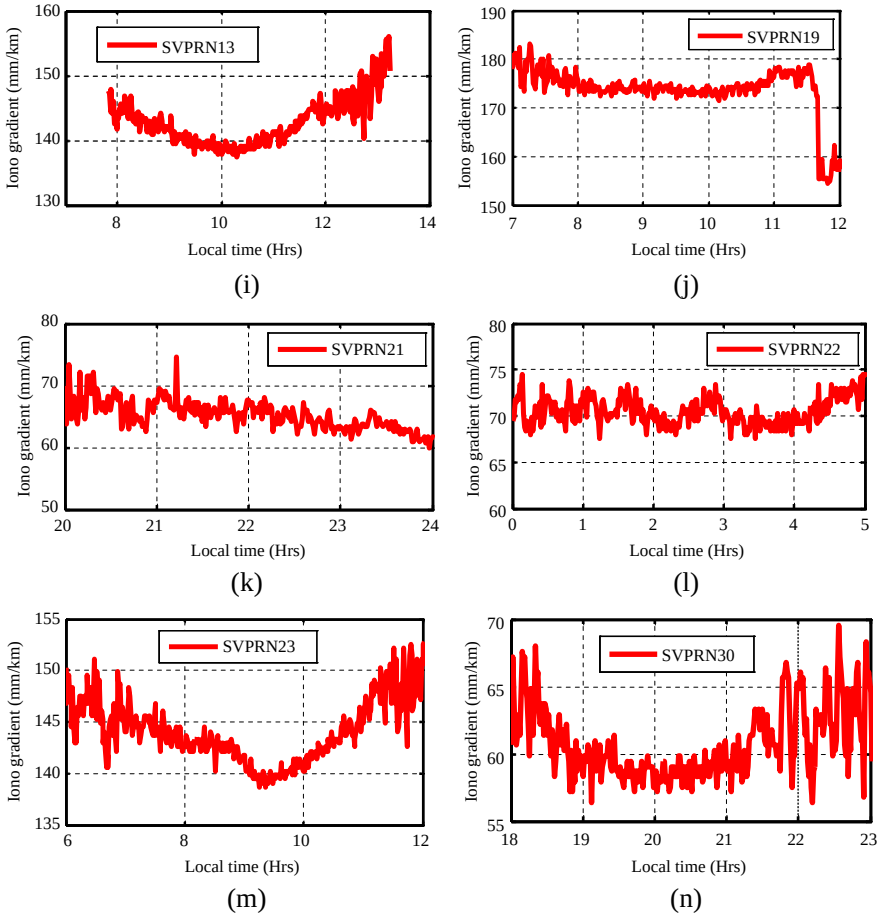

Figure 9. Slant ionospheric spatial gradients of SVPRNs during normal ionospheric conditions on 2nd October 2008. (a) SVPRN3, (b) SVPRN4, (c) SVPRN6, (d) SVPRN8, (e) SVPRN9, (f) SVPRN10, (g) SVPRN11, (h) SVPRN12, (i) SVPRN13, (j) SVPRN19, (k) SVPRN21, (l) SVPRN22, (m) SVPRN23, and (n) SVPRN30.

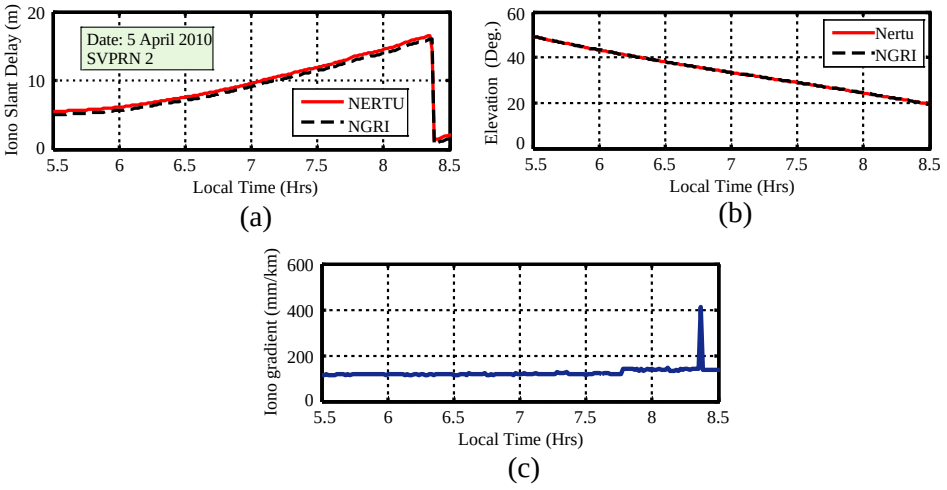

Figure 10. Plots showing local time versus (a) slant ionospheric delay, (b) elevation angle, (c) ionospheric spatial gradient of SVPRN 2 on 5th April 2010.

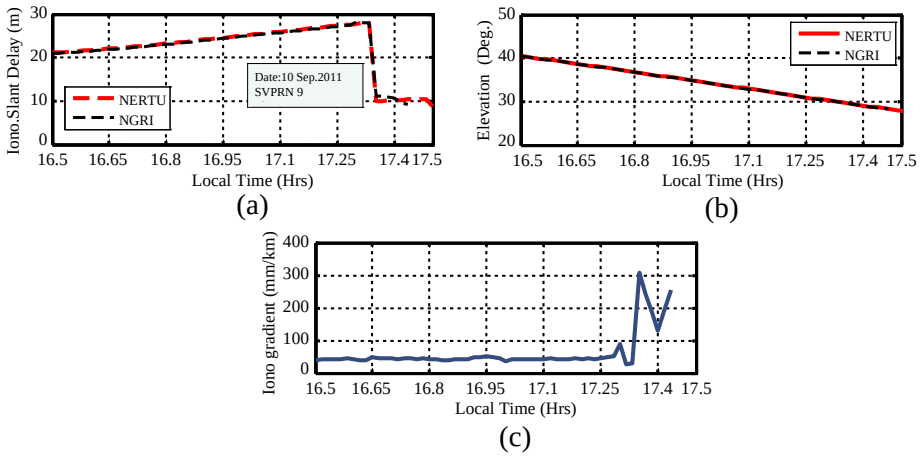

Figure 11. Plots showing local time versus (a) slant ionospheric delay, (b) elevation angle, (c) ionospheric spatial gradient of SVPRN 9 on 10th September 2011.

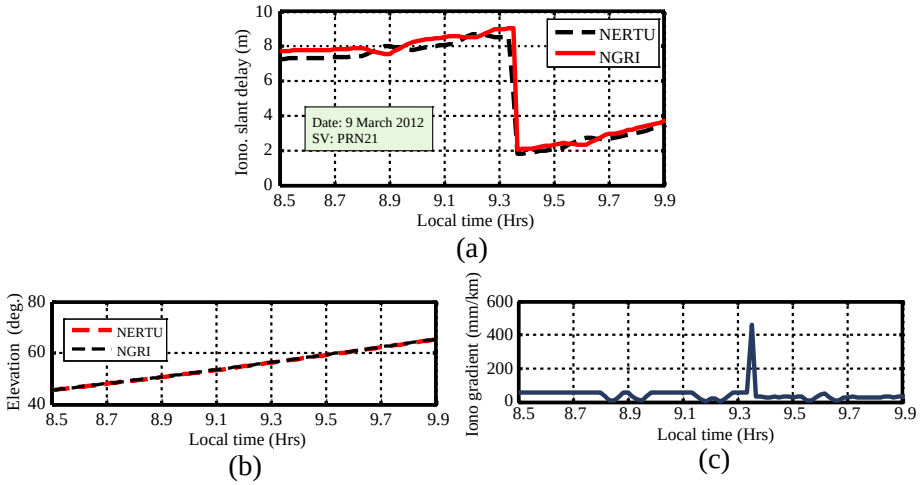

Figure 12. Plots showing local time versus (a) slant ionospheric delay, (b) elevation angle, (c) ionospheric spatial gradient of SVPRN 21 on 9th March 2012.

value is 1 at an elevation angle of 90° and 3.0 at an angle of 5°. Therefore, it is evident from the above results that the slant ionospheric spatial gradients are large enough and can result σ_{vig} greater than 4 mm/km as prescribed by ICAO for LAAS operations even under normal ionospheric conditions (RTCA, 2005). The identified large spatial gradients can impose severe threat to the LAAS users and is dealt in following section. The magnitude of anomalous gradients noticed with our data is compared with that due to GPS data over CONUS region. More precisely, the observations presented correspond to the ionospheric data analysed during the intense inosopheric activity days. The large spatial gradients are noticed on 5th April 2010 ($3 \leq \text{Kp} \leq 8$), 10th September 2011 ($3 \leq \text{Kp} \leq 6$) and 9th March 2012 ($2 \leq \text{Kp} \leq 8$). Figures 10–12 depict the results of gradient effected satellite PRNs on the respective days. Table 2 gives the values of the calculated threat space parameters such as velocity of wave front, width and direction of the wave front etc., to quantify the effect of gradients on the satellites mentioned. The maximum ionosphere slope of 460.4 mm/km (9th March 2012) in slant domain is observed over a distance of approximately 4 km. The maximum anamolous ionospheric gradient reported using WAAS and IGS/CORS networks over CONUS region is 355.74 mm/km between the stations WOOS (Lat: 40.80°, Long: −81.96°) and GARF (Lat: 41.42°, Long: −81.61°) separated by a distance of 74.51 km [25]. But, at low latitudes, the decorrelation of ionosphere is comparatively large,

Table 2. Ionospheric threat parameters estimated for gradient effected SVs PRN 2, 9 and 21 on 5th April 2010, 10th September 2011 and 9th March 2012 respectively.

S. No	Date	SV PRN	g_s (mm/km)	Vig (mm/km)	LT (Hrs)	V_{iono} (m/sec)	W_{iono} (km)	θ_{iono} (deg.)
1.	5th Apr. 2010	2	409.3	189.49	8.36	151.87	7.28	23.17
2.	10th Sep. 2011	9	306.7	175.25	17.35	147.21	7.28	24.65
3.	9th Mar. 2012	21	460.4	396.9	9.35	106.06	10.92	38.32

this is evident from the data analysis. Any further comparison based on other observations/parameters is not possible as this type of work, particularly in the context of LAAS is done for the first time in low latitude region.

Usually, the methodology adopted for threat analysis is capable of identifying only the moving ionospheric gradients and their impact on the GPS signals but not the stationary gradients (Sections 4.1–4.4). However, there is a possibility of stationary ionospheric gradients, which require through investigation. The effect of stationary gradients are considered as worst case scenario and can be mitigated through geometry screening, with MIEV as key deciding factor [14]. This is achieved by

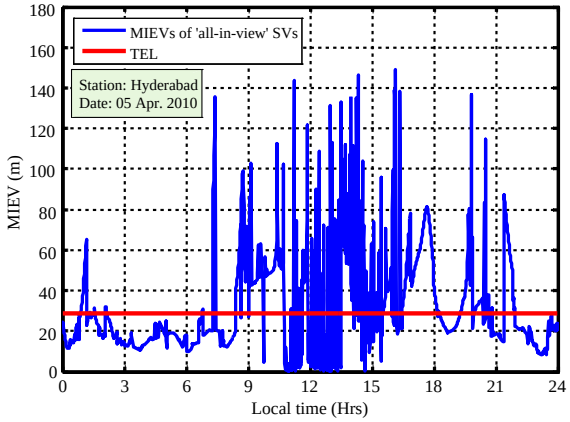

Figure 13. MIEV for 'all-in-view' satellites on 5th April 2010.

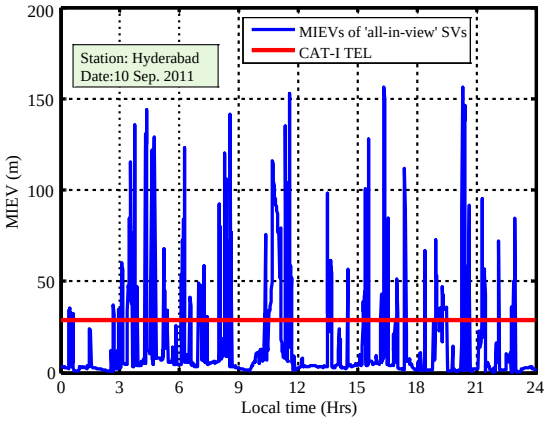

Figure 14. MIEV for 'all-in-view' satellites on 10th September 2011.

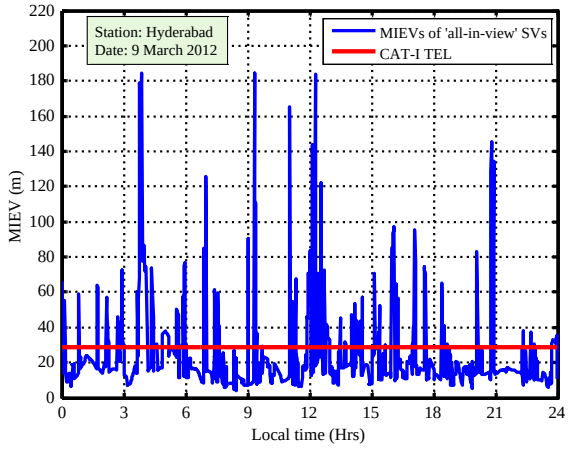

Figure 15. MIEV for 'all-in-view' satellites on 9th March 2012.

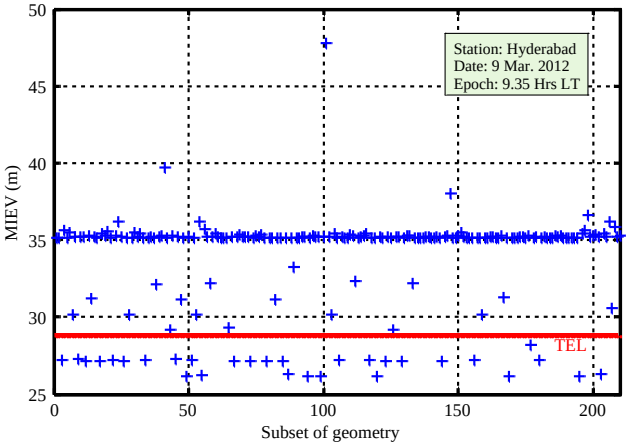

Figure 16. MIEVs for subset of satellite geometries (9th March 2012 at 9.35 Hrs LT).

calculating the MIEV for the 'all-in-view' visible satellites at every epoch. The all-in-view satellites with MIEV less than CAT-I TEL of 28.8 m are considered for position estimation. Otherwise, the geometry screening is carried out, where nC_4 combinations of satellite subsets are generated and the subset with MIEV less than CAT-I TEL is used for navigation solution. The MIEVs calculated for the aforesaid days are depicted in Figures 13–15. It is observed that, there are several satellite geometries with MIEVs exceeding the TEL. The large MIEV values indicate the presence of stationary gradients. The potential integrity risk due to satellite geometries exceeding TEL are mitigated through geometry screening at those epochs.

For example, Figure 16 shows the MIEVs obtained for nC_4 combinations at an epoch (9.35 Hrs LT) on 9th March 2012 for which the MIEV is 184.4 m due to 'all-in-view' satellites. At this epoch, it is observed that the number of total visible satellites are '11' (SV PRN 1, 3, 6, 11, 14, 16, 20, 21, 30, 31 and 32) at this epoch. Thus, 210 geometries are possible. MIEVs are calculated for these 210 combinations (Figure 16). It is observed that MIEV crosses the TEL for 180 combinations out of 210 combinations. Thus the 180 satellite combinations are unsafe to the LAAS user. So, these combinations are not used by airborne GBAS avionics for navigation solution.

6. CONCLUSIONS

The maximum slant ionospheric gradient observed is 460 mm/km from the threat analysis carried out using the GPS data of NERTU and NGRI stations. Further analysis of MIEVs not only aids in providing the safe satellite geometry for airborne GBAS avionics, but also reveals the presence of stationary ionospheric gradients and their impact on the signals. It is noticed that most of the time the MIVE values exceed the CAT-I TEL of 28.8 m. The MIEV values are critical for estimating inflation factor to determine HPL and VPL for an intended flight operation. Due to the constraint of limited data, the calculations are done based on assumptions reported elsewhere [14]. The analysis is useful for development of ionospheric storm warning and alert monitoring systems. In addition, the effect of stationary gradients is mitigated using geometry screening (nC_4) and safe satellite subsets are identified.

ACKNOWLEDGMENT

The research work presented in this paper has been carried out under the DST, New Delhi sponsored project vide sanction letter No. SR/S4/AS-89/2012, dated: 25th September 2012.

REFERENCES

1. Venkata Ratnam, D., A. D. Sarma, V. Satya Srinivas, and P. Sreelatha, "Performance evaluation of selected ionospheric delay models during geomagnetic storm conditions in low-latitude region," *Radio Science*, Vol. 46, No. 3, RS0D08, 2011.
2. Satya Srinivas, V., A. D. Sarma, K. C. T. Swamy, and K. Satyanarayana, "Performance evaluation of IRI-2007 at equatorial latitudes and its matlab version for GNSS applications," *Advanced Space Research Journal*, Vol. 52, No. 10, 1845–1858, Elsevier, 2013.
3. Swamy, K. C. T., A. D. Sarma, V. Satya Srinivas, P. Naveen Kumar, and P. V. D. Somasekhar Rao, "Accuracy evaluation of estimated ionospheric delay of GPS signals based on Klobuchar and IRI-2007 models in low latitude region," *IEEE Geoscience and Remote Sensing Letters*, Vol. 10, No. 6, 1557–1561, 2013.
4. Ravichandra, K., V. Satya Srinivas, and A. D. Sarma, "Investigation of ionospheric gradients for GAGAN applications," *Earth Planets Space Journal*, Vol. 61, 633–635, 2009.
5. Parkinson, B. W. and J. J. Spilker, *Global Positioning System: Theory and Applications*, Vol. 1, American Institute of Aeronautics and Astronautics, Washington, 1996.
6. Walter, T., S. Datta-Barua, J. Blanch, and P. Enge, "The effect of large ionospheric gradients on single frequency airborne smoothing filters for WAAS and LAAS," *Proceedings of ION NTM*, 490–501, Jan. 2004.
7. ICAO, "Aviation system block upgrades," Working Document, Nov. 2011.

8. ICAO, "Validated ICAO GNSS standards and recommended practices (SARPS)," Nov. 2000.
9. Christie, J. R. I., P. Y. Ko, A. Hansen, D. Dai, S. Pullen, B. Pervan, and B. Parkinson, "The effects of local ionospheric decorrelation on LAAS: Theory and expreimental results," *Proceedings of the Institute of Navigation, National Technical Meeting*, 769–777, 1999.
10. Pullen, S., Y. S. Park, and P. Enge, "Impact and mitigation of ionospheric anomalies on ground-based augmentation of GNSS," *Radio Science*, Vol. 44, No. 1, 2009.
11. Lee, J., M. Luo, S. Pullen, Y. S. Park, and P. Enge, "Position-domain geometry screening to maximize LAAS availability in the presence of ionosphere anomalies," *ION GNSS 19th International Technical Meeting, Satellite Division*, 393–408, Fort Worth, Tx, Sep. 26–29, 2006.
12. Datta-Barua, S., T. Walter, S. Pullen, M. Luo, J. Blanch, and P. Enge, "Using WAAS ionospheric data to estimate LAAS short baseline gradients," *Proceedings of ION National Technical Meeting*, 523–530, Anaheim, CA, Jan. 28–30, 2002.
13. Luo, M., S. Pullen, T. Walter, and P. Enge, "Ionosphere spatial gradient threat for LAAS: Mitigation and tolerable threat space," *Proceedings of ION NTM*, 490–501, 2004.
14. Lee, J., J. Seo, Y. S. Park, S. Pullen, and P Enge, "Ionospheric threat mitigation by geometry screening in GNSS ground based augmentation systems," *Journal of Aircraft*, Vol. 48, No. 4, 1422–1433, 2011.
15. Ramakrishnan, S., J. Lee, S. Pullen, and P. Enge, "Targeted ephemeris decorrelation parameter inflation for improved LAAS availability during severe ionospheric anomalies," *Proceedings of ION NTM*, 354–366, 2008.
16. Rife, J. and R. E. Phelts, "Formulation of a time-varying maximum allowable error for ground-based augmentation system," *IEEE Transactions on Aerospace and Electronics Systems*, Vol. 44, No. 2, 548–559, Apr. 2008.
17. Murphy, T., "Considerations for GBAS service levels to support CAT II/III precision approach," *ICAO GNSSP-WP-19 Meeting*, Yokohama, Oct. 2000.
18. RTCA, "Minimum operational performance standards for GPS local area augmentation system airborne equipment," RTCA-DO-253A, Nov. 2001.
19. ICAO Annex 10, "International standards and recommended practices — Aeronautical telecommunications," Vol. I, Radio Navigation Aids, Amendment 77, 2010.
20. Konno, H., "Dual-frequency smoothing for CAT III LAAS: Performance assessment considering ionosphere anomalies," *ION GNSS 20th International Technical Meeting, Satellite Division*, 424–437, Fortwworth, TX, Sep. 25–28, 2007.
21. Mcgraw, G. A., T. Murphy, M. Brenner, S. Pullen, and A. J. Van Dierendonck, "Development of the LAAS accuracy models," *Proceedings of ION GPS*, 1212–1223, Salt Lake City, UT, Sep. 19–22, 2000.
22. Rowson, S., K. Van Dyke, P. Kline, T. Murphy, and Q. Hua, "Evaluation of LAAS availability with an enhanced GPS constellation," *IEEE Position Location and Navigation Symposium*, 501–509, 1998.
23. Lee, J., S. Pullen, S. Datta-Barua, and P. Enge, "Assessment of ionosphere spatial decorrelation for global positioning system-based aircraft landing systems," *AIAA Aircraft Journal*, Vol. 44, No. 5, 1662–1669, 2007.
24. Datta-Barua, S., J. Lee, S. pullen, M. Luo, A. Ene, D. Qiu, G. Zhang, and P. Enge, "Ionosphere threat parameterization for local area global positioning system-based aircraft landing system," *Journal of Aircraft*, Vol. 47, No. 4, 1141–1151, Jul.–Aug. 2010.
25. Ene, R., D. Qiu, M. Luo, S. Pullen, and P. Enge, "A comprehensive ionosphere storm data analysis method to support LAAS threat model development," *Proceedings of National Technical Meeting of The Institute of Navigation*, 110–130, San Diego, CA, Jan. 2005.
26. Pottmann, H. and W. Johannes, *Computational Line Geometry*, Springer Verlag, Heidelberg, Berlin, 2001.